Mekanika: Majalah Ilmiah Mekanika

.

Performance Analysis of the Fast Platform Supply Vessel with a Conventional V-Hull Shape with the Addition of a Chine and a Different Bow Using Computational Fluid Dynamics Method

Fedrik Immanuel Rumapea[1], Aldias Bahatmaka[1]*, Banin Hamizan[1], Pramudya Rahardian[1], Umar Zaid Rantisi[1], Dias Fitria Kurniaputri[1]

1 Department of Mechanical Engineering, Universitas Negeri Semarang, Semarang, Indonesia

* Corresponding Author's email address: aldiasbahatmaka@mail.unnes.ac.id

Keywords:
Ship
Platform supply
CFD
V hull

Abstract
Indonesia is the largest country in Southeast Asia, consisting of more than 17,000 islands and a coastline of approximately 81,000 kilometers, with over half of its territory covered by water. To optimize this vast marine potential for public welfare, comprehensive data collection and mapping are essential. The oil and gas sector remains a key contributor to national revenue. For instance, Pertamina Hulu East Kalimantan (PHKT) exceeded its 2023 production target, achieving around 9,900 barrels of oil and 45 million cubic feet of gas per day. To support offshore operations, a Platform Supply Vessel (PSV) prototype named Bramantya was designed. This study analyzes the vessel using Computational Fluid Dynamics (CFD) to determine the optimal hull form for operational performance and fuel efficiency. Three hull variations were examined: a conventional hull, a hull with additional chines, and a wide-bow hull. The simulation was validated against previous experimental studies, showing consistent linear results with an average error of 4.25%. Simulations at Froude numbers 0.2–0.6 show that the wide downward-bowed hull reduces drag by 7.69% compared to the conventional hull, thereby improving fuel efficiency.

1 Introduction

Indonesia is the largest country in Southeast Asia and has the largest maritime archipelago in the world by area [1]. Its coastline stretches 81,000 km. Approximately 70% of Indonesia's territory comprises 17,000 islands and maritime areas. Indonesia's maritime territory covers 2.7 million km^2 of the Indonesian Exclusive Economic Zone (EEZ) and 3.1 million km^2 of sovereign waters [2]. According to statistics, 64.97% of Indonesia's total territory is water [3]. With such a vast ocean, this certainly means important consequences that must be addressed immediately, namely, conducting a comprehensive inventory and mapping. This is necessary so that all potential natural resources can be properly identified and utilized as national natural resources to improve the welfare of the people [4].

Oil and natural gas continue to play a significant role in generating foreign exchange and contributing to the Indonesian economy. Since oil and gas are key resources for economic development, they must be

https://dx.doi.org/10.20961/mekanika.v25i1.114601

Revised 17 March 2026; received in revised version 20 March 2026; Accepted 21 March 2026
Available Online 30 April 2026

2579-3144

managed prudently and under strict regulation. Among Indonesia's oil and gas resources, the "X" field in East Kalimantan is significant due to its substantial production and economic impact. The following data on offshore oil and gas production in East Kalimantan Province is based on the Energy and Mineral Resources Service of East Kalimantan Province, as shown in Table 1.

Table 1. East Kalimantan oil and gas production data

Oil and Gas Production	2019	2020	2021
Oil (barrel)	21038829	19296864.23	17742360
Gas (MMBTU)	231067411	203955179.69	172829530

Pertamina Hulu East Kalimantan (PHKT) is one of the operators of Offshore Oil and Gas Exploration and Exploitation activities in East Kalimantan. Pertamina Hulu East Kalimantan (PHKT) officially managed the East Kalimantan Working Area (WK) from October 25, 2018, until the end of the contract in 2038. PHKT's fields include Attaka, Sepinggan, Yakin, Melahin, Sapi, Kerindingan, Santan, Seguni, Sejadi, Seturian, Mahoni, Pantai, Lawe-Lawe, and Bangkirai. In 2023, PHKT produced an average of 9.9 thousand barrels of oil per day (MBOPD) and 45 million standard cubic feet of gas per day (MMSCFD) [5]. With so many fields managed by PHKT, a fleet of vessels is required to support exploration and exploitation activities, including Platform Supply Vessels (PSVs). A Platform Supply Vessel is a specialized type of vessel used to supply rig and platform supplies [6]. Platform Supply Vessels have excellent maneuverability to operate around rigs and platforms, enabling them to fulfill supply chain requirements and reliably provide operational support in offshore waters [7].

Although maritime transportation is vital to regional economic growth, this industry faces significant environmental challenges due to the impact of the use of High Sulfur Fuel Oil (HSFO) [8]. The maritime transportation sector is a major contributor to conventional pollutants and greenhouse gases, with estimates that this sector contributes around 3% of GHG emissions [5]. The maritime transportation sector has numerous environmental impacts, such as noise pollution from ship engines and air pollution originating from exhaust emissions in the form of NOx, SOx, Particulate Matter, CO, and CO2 [9]. These compounds cause environmental problems, acid rain, greenhouse gas emissions, and even human health, particularly the respiratory system [10]. Therefore, it is crucial to reduce emissions from the maritime transportation sector.

In the context of the push towards a cleaner energy market, the IMO has regulated the prohibition of the use of marine fuel with a sulfur content higher than 0.5% [5]. To support this regulation, Indonesia, through the Ministry of Transportation, issued Ministerial Regulation Number PM 29 of 2014. Article 36 of this regulation sets a limit on the sulfur content in marine fuel of 0.5%, which came into effect on January 1, 2020. Furthermore, the Director General of Sea Transportation issued Circular Letter Number UM.003/93/14/DJPL-18 on October 30, 2018, which regulates the sulfur content limit in fuel and the obligation to report fuel consumption on ships [11].

Achieving minimum drag is a crucial issue in ship design. Numerous approaches can be employed, including hull optimization or the selection of a different bow [12]. Through computational fluid dynamics, Le et al. explored how variations in bow geometry, specifically blunt and rounded shapes, affect ship resistance [13, 14]. The use of a hull with additional chines is intended to increase the ship's stability in open-sea waves. The widened bow is an effort to reduce resistance in seawater. However, several drawbacks, such as lower buoyancy, cause the ship to tend to press underwater and make the deck very wet because the shape does not expand laterally [15].

White et al. investigated the hydrodynamic performance of the effect of an inverted bow on the drag and seakeeping capabilities of the hull shape of a Navy Combat Ship using experimental methods [16]. Nazemian and Ghadimi optimized the inverted-bow geometry of a rounded trimaran hull using numerical

analysis to reduce drag [17]. This research compared the influence of incorporating a chine and extending a wide bow downward against a conventional V-shaped hull, focusing on the resistance range corresponding to Froude numbers between 0.2 and 0.6. The analysis used a CFD framework based on the RANS equations, with the Shear Stress Transport (SST) model for turbulence modeling.

This simulation aims to compare the performance of three hull concepts: a hull with an additional chine, a wide-bow hull, and a conventional hull, to determine which is most effective in reducing drag. Previously, research has often focused on a single type or only on high speeds. This study instead tested all three at a wider range of speeds, including the medium speeds often used in daily operations. Furthermore, the analysis aims to look at the total drag figure, which is the main cause of increased fuel consumption. Simply put, we not only know which is "more economical" but also understand "why and under what conditions" a particular hull design excels. These findings are expected to provide a more practical and in-depth guide for offshore companies in selecting the most efficient and economical design for their operational needs.

2 Model and Boundary Methods

The preparation of this study begins with the following stages: determining the dimensions of the ship prototype used in this simulation, as shown in Table 1, and depicting the hull configuration in Figure 1. The hull variations in Figure 1 show the conventional hull 1(a), the hull with a chine 1(b), and the hull with a wide bow 1(c). All ship dimensions are set to the same values in the Maxsurf modeler, and the following hull data are obtained: Length overall (LOA), displacement, and water surface area, as shown in Table 2. In this analysis, hull resistance is evaluated for speeds at the Froude numbers listed in Table 3.

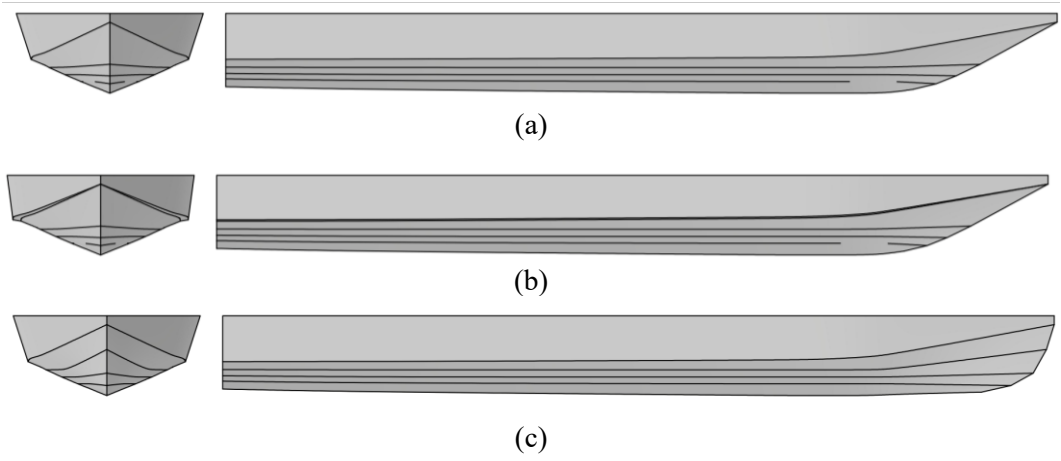

Figure 1. Hull types: (a) conventional hull, (b) hull with chine, and (c) hull with a wide bow downwards

Table 2. Hull dimension details

Dimension	Conventional Hull	Hull with Chine	Hull with a Wide Bow Downwards
Length overall (LOA)	2 m	2 m	2 m
Length waterline (LWL)	1.85 m	1.85 m	1.97 m
Beam	0.45 m	0.45 m	0.45 m
Deep	0.19 m	0.19 m	0.19 m
Draft	0.09	0.09	0.09
Displacement	30.99 kg	31.74 kg	31.32 kg
Wetted Area	0.718 m^2	0.768 m^2	0.748 m^2
RT @Fn 0.5	18.87 N	26.47 N	17.82 N
RT/Displacement	0.61 N/kg	0.83 N/kg	0.57 N/kg

CT (×10⁻³) @Fn 0.5	4.21	5.52	3.82

Table 3. Froude number variations

Froude	Speed (m/s)
0.2	1.252836781
0.3	1.879255172
0.4	2.505673562
0.5	3.132091953
0.6	3.758510343

Although there are differences in displacement and length-waterline (LWL) values among the three hull models, these are a natural consequence of modified hull geometry and reflect the actual conditions under which designs with the same main dimensions are operated. To ensure a fair comparison, this study uses several approaches: Normalization by coefficient of resistance (CT) to accommodate differences in wetted surface area, Resistance analysis per unit displacement to evaluate the relative efficiency of each design in moving its ship mass, Controlled trim conditions at even keel (0°) for all simulations, so that differences in wave resistance are solely due to hull shape, not by different ship attitudes.

Fluid flow simulations based on the RANS equations employ a predictor–corrector scheme that couples the continuity and turbulence equations with the Shear Stress Transport (SST) $k-\omega$ model. This model was chosen because it combines the robust and accurate formulation of the $k-\omega$ model in the near-wall region with the free-stream independence of the $k-\epsilon$ model, making it well-suited to capturing free-surface effects and flow separation associated with ship resistance. This approach is also in accordance with the International Towing Tank Conference (ITTC) recommendations for high-fidelity ship CFD applications [18]. The structure of the RANS equations includes three fundamental steps:

1. Combining the formulas governing fluid motion throughout the control area of the solution domain.
2. Splitting the integral formula into a set of algebraic equations.
3. The algebraic equations are solved iteratively by applying the RANS formulation in combination with numerical turbulence modeling. The discretization is performed using the finite volume method, followed by solution management via the SIMPLE algorithm and the Hidden Pressure Adjustment technique, applied to the flow rate and pressure equations, respectively.

The effect of the free surface is explained by a method known as "Volume-of-Fluid": the assumption that the solution domain consists of a sufficient amount of fluid, whose properties vary with volume fraction, as shown in equation (1). In Computational Fluid Dynamics, it is assumed that the volume fraction of fluid in each cell is represented by a function, F, whose value is one for a cell completely filled with water, while a value of zero indicates the absence of water. Therefore, any fluid with a value between 0 and 1 must have a free surface. The shape of the free surface can be described by the conservative transport equation presented in Equation 1.

$$\frac{\delta F}{\delta t}+\frac{\delta uF}{\delta x}+\frac{\delta vF}{\delta y}+\frac{\delta wF}{\delta z}=0 \quad \text{.....(1)}$$

This study treats the ITTC as a global standard for predicting shipboard fluid dynamics using both numerical and experimental methods. In the case of high-speed ships, the ITTC suggests several aspects, including [18]:

1. Dimensions of the computational area and constraint conditions
2. Grid size
3. Convergence process

4. Time interval

Figure 2 shows the size of the computational area and its limitations. The hull of the ship is placed in a beam space with dimensions from the bow to the front of 1 LOA, from the stern to the rear of 2.5 LOA, from the deck upwards of 1 LOA, from the hull downwards of 2 LOA, and from the side of the hull to the boundary conditions is 1.5 LOA [19,20].

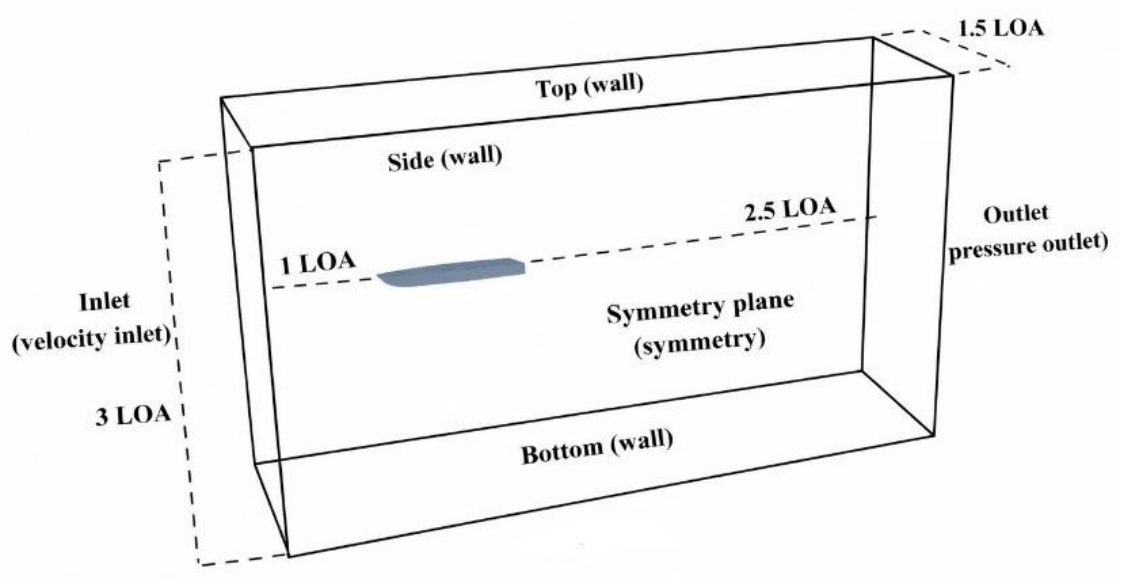

Figure 2. Boundary conditions for the current study

Next, let's discuss the limitations. The inlet velocity is directed along the negative x-axis, which corresponds to the region where the wave simulation is conducted. Conversely, the positive x-direction is assigned as the outlet pressure boundary, reflecting the static pressure at the outflow location. The walls define the upper and lower boundaries of the domain. To optimize computational time, the simulation is performed on half of the ship's hull, utilizing symmetry along the centerline [21]**.**

In this study, meshing is a crucial step to ensure the accuracy of hydrodynamic simulations. Given the high computational cost, especially for simulations with a large number of elements, a mesh convergence analysis is mandatory to determine the optimal grid resolution, the one that provides adequate accuracy while remaining computationally efficient [22]. A mesh independence study was conducted on the conventional hull for two Froude number conditions: Fn = 0.2 (low speed) and Fn = 0.5 (medium-high speed). The selection of Fn = 0.5 is critical because, at this speed, the wave-making resistance component begins to dominate, making the mesh resolution at the free surface and bow areas particularly important. Seven mesh levels with increasing node counts were generated, as shown in Table 4.

Table 4. Mesh independence study and Grid Convergence Index (GCI) calculation at Fn = 0.2 and Fn = 0.5

Number of Nodes	Total Resistance Fr 0.2	Difference (%) Fr 0.2	Total Resistance Fr 0.5	Difference (%) Fr 0.5
290879	4.99	-3.19	27.91	-1.83
613538	4.58	-8.29	27.34	-2.02
993861	4.10	-10.51	26.80	-1.96
1235106	3.67	-10.36	26.05	-2.82
1784944	3.23	-12.14	26.47	1.63
2045573	3.26	1.16	26.51	0.14

To quantify the numerical uncertainty due to mesh discretization, the Grid Convergence Index (GCI) method based on Richardson Extrapolation was applied, following the procedures recommended by ITTC [18]. The GCI provides an upper bound on the relative numerical error with respect to the asymptotic convergent value. The results of the GCI calculation for total resistance (RT) at both Froude numbers are presented in Table 4. If more nodes were selected, the simulation time would be longer, although the final results would not differ much [23]. From Table 4, it is evident that the resistance values begin to converge with a mesh of 1,784,944 nodes. The GCI calculation shows that for this mesh, the numerical uncertainty relative to the finer mesh (2,045,573 nodes) is very small: 2.38% at Fn 0.2 and 2.95% at Fn 0.5. This GCI value, below 5%, indicates that the 1,784,944-node mesh has achieved excellent convergence and high accuracy [23]. Further increasing the number of nodes to 2,045,573 results in a resistance change of only 1.16% at Fn 0.2 and -0.14% at Fn 0.5, with the GCI value dropping drastically, confirming that the solution has entered the asymptotic convergence range. Therefore, the mesh with 1,784,944 nodes was selected as the best compromise between accuracy and computational efficiency for all subsequent simulations across all speed variations and hull types.

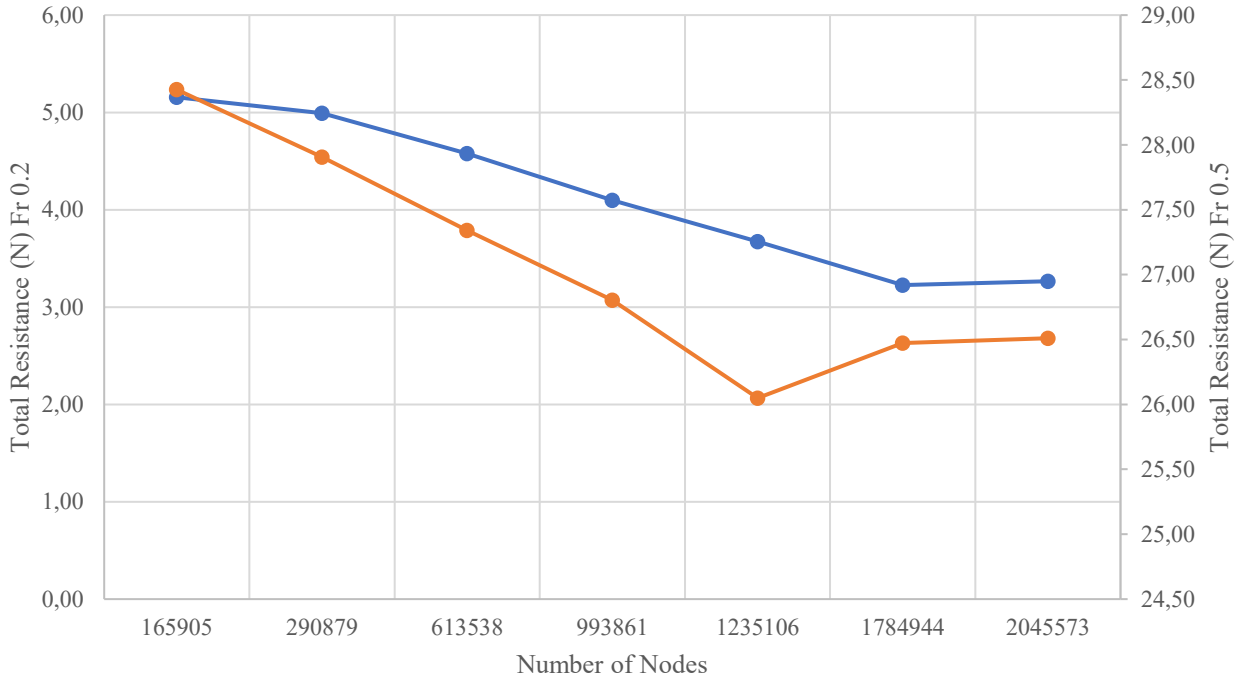

Figure 3. Visualization of mesh convergence at Fn = 0.2 and Fn = 0.5.

In this simulation, meshing plays an important role in ensuring the accuracy of hydrodynamic simulations [24]. The mesh sizes are shown in Figure 4 to observe the impact of hull variations and mesh counts. The grid size on the hull is increased to obtain more precise measurements of the ship's motion dynamics. Figure 4 shows the grid size from the side. This simulation uses a hexahedral structured mesh, which offers significant advantages, particularly in terms of computational efficiency and numerical accuracy. According to Tucker's research, hexahedral structured meshes tend to produce lower discretization errors compared to unstructured meshes for an equivalent number of cells, because the regularity of the cell geometry maintains the accuracy of higher-order numerical schemes [25]. In addition, the ability to precisely control grid stretching and aspect ratio, especially in the boundary layer region, makes it an ideal choice for turbulent flow simulations with stringent near-wall resolution requirements, such as those often used in Reynolds-Averaged Navier-Stokes (RANS) modeling [26,27].

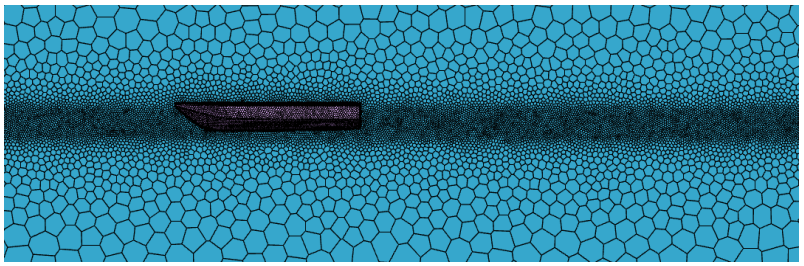

(a)

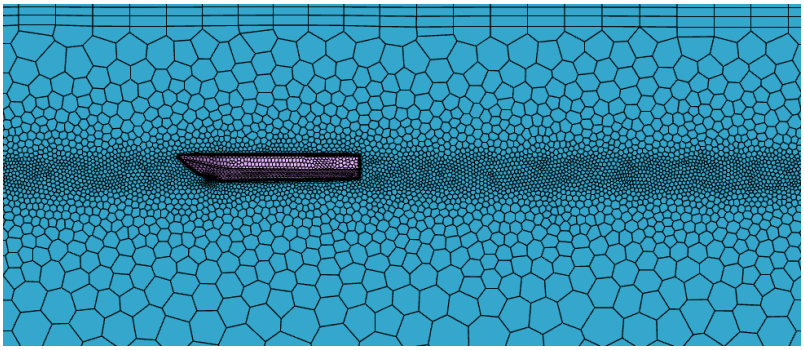

(b)

Figure 4. Meshing side view: (a) 2045573 number of nodes, and (b) 165905 number of nodes

To ensure the accuracy of the SST $k-\omega$ model, with particular attention to the near-wall mesh resolution. As shown in the mesh configuration (Figure 4), prism layers were generated to maintain a y^+ value close to 1 on the hull surface. This resolution allows the solver to resolve the viscous sublayer directly, avoiding less accurate wall functions and ensuring the boundary layer is captured correctly, which is critical for predicting frictional resistance.

The time step determines the temporal resolution for each iteration in the unsteady RANS simulation. In this study, a non-dimensional time step is formulated as Equation 2.

$$\Delta t^* = \Delta t \cdot \frac{V}{L} \quad \text{.....(2)}$$

with Δt^* is a non-dimensional time step, Δt is physical time step (in seconds), V is ship speed, L ship length, then time step 0.5 was applied, following the recommendations of ITTC (2011) for ship resistance predictions. This value has been successfully employed in previous CFD studies on similar hull forms [19-21] and ensures that the Courant-Friedrichs-Lewy (CFL) number remains below unity in the majority of the computational domain, particularly in regions with high velocity gradients near the hull surface [21, 28,29].

The CFL condition was monitored throughout all simulations, with the finest mesh resolution of approximately 0.019 m in the near-wall region and an applied time step of 0.5; the maximum CFL number was consistently maintained below 0.85 across all Froude numbers from 0.2 to 0.6, as formulated in Equation 3.

$$CFL = \frac{V\Delta t}{\Delta x} \quad \text{.....(3)}$$

With Δx is mesh resolution. This is well within the stability limits for the implicit pressure-based solver used in ANSYS CFX [22].

Although the theoretically optimal time step may vary with vessel speed, the use of a constant non-dimensional time step is justified by the implicit time-marching scheme, which offers greater numerical stability and permits larger time steps without sacrificing accuracy [27]. More importantly, the validity of

the chosen time step is indirectly confirmed by the successful validation against experimental data, which showed excellent agreement with an average error of only 4.25% (see Figure 5 and Table 5). This close correlation with benchmark experimental results demonstrates that the combination of mesh resolution, turbulence model, and time step employed in this study is sufficient to accurately capture the hydrodynamic resistance characteristics of the investigated hull forms.

3 Results and Discussion

3.1 CFD verification

In this simulation, CFD validation was carried out on Nasirudin's research, and validation in this study used a stomach with a chine-type hull. The validation results showed the largest difference, at 6.1%. Figure 5. Validation of the present CFD setup (using SST $k-\omega$ turbulence model) against experimental data from Nasirudin et al. [13]. Results from numerical simulations and experimental analyses showed similar patterns. However, there were some variations between the CFD and experimental results due to limitations in CFD modeling, which do not fully reflect real-world conditions. This research also aligns with a study by Brizzola and Serra. They explored the accuracy of numerical simulations in predicting ship design. They found variations in drag values and compared them with Savitsky's experimental data [30], which results in an average error of about 10% in the resistance forecast [31]. Table 5 shows the percentage difference between the experimental results conducted by Nasirudin et al. and the CFD analysis. Figure 6 shows the convergence history during the simulation.

Table 5. Validation results

Froude	Nasirudin et al. [13] (N)	CFD (N)	Error (%)
0.2	3.04	3.23	6.13
0.3	9.64	9.31	-3.44
0.4	18.28	17.58	-3.80
0.5	27.32	26.47	-3.1
0.6	32.22	30.68	-4.79

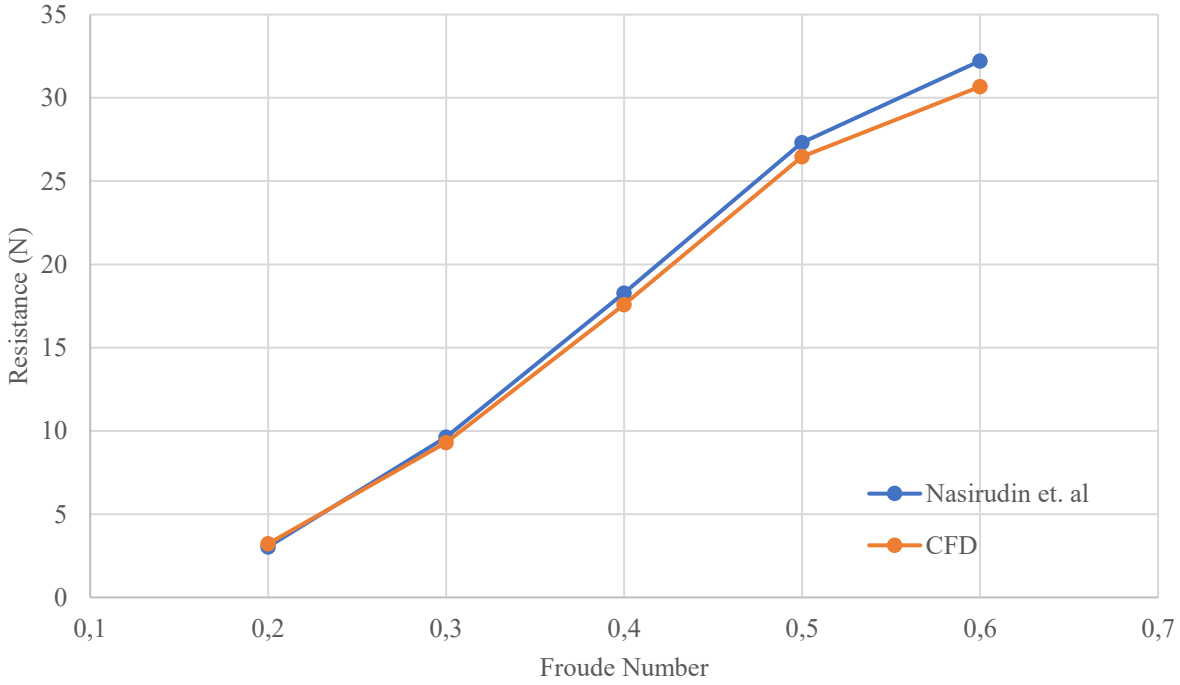

Figure 5. Validation graph comparison

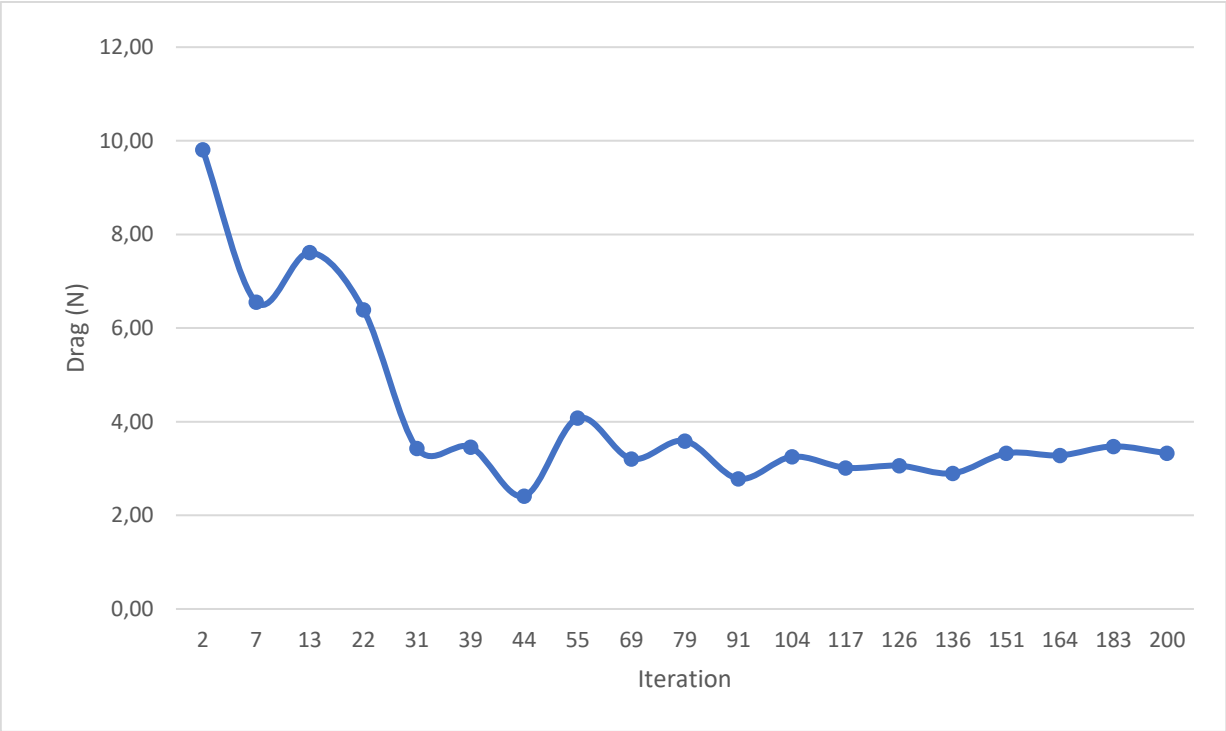

Figure 6. Convergence history

3.2 Numerical simulation

The resistance results for the conventional hull and the chine hull in this experiment are presented in Figure 7, and Table 6 shows the total resistance of both hull types, each at ship speeds measured by the Froude number Fr. The difference in resistance between the chine hull and the conventional hull is also presented. The chine hull exhibits higher resistance compared to the conventional hull, with an average difference of about 20.7%. The explanation for this is that the chine water area is larger than a conventional hull. Regarding total resistance (Figure 7 and Table 6), at all ship speeds the chine hull exhibits higher total resistance than the conventional hull, with an average difference of about 20.7%. This indicates that the chine hull is less efficient in terms of engine power savings compared to the conventional hull. Based on the results obtained, the stability of the chine hull is better than that of the conventional hull. This is caused by the chine expanding the waterplane area when the ship is upright, so that the metacentric height (GM) increases. The chine also causes a sudden change in the waterplane area, which provides additional "lift" to keep the ship upright when it is tilted.

Table 6. Resistance results: conventional hull vs. hull with chine

Froude	Conventional Hull (N)	Hull with Chine (N)	Error (%)
0.2	3.09	3.23	4.52
0.3	9.09	9.31	2.36
0.4	16.23	17.58	8.33
0.5	18.88	26.47	40.23
0.6	20.71	30.68	48.13

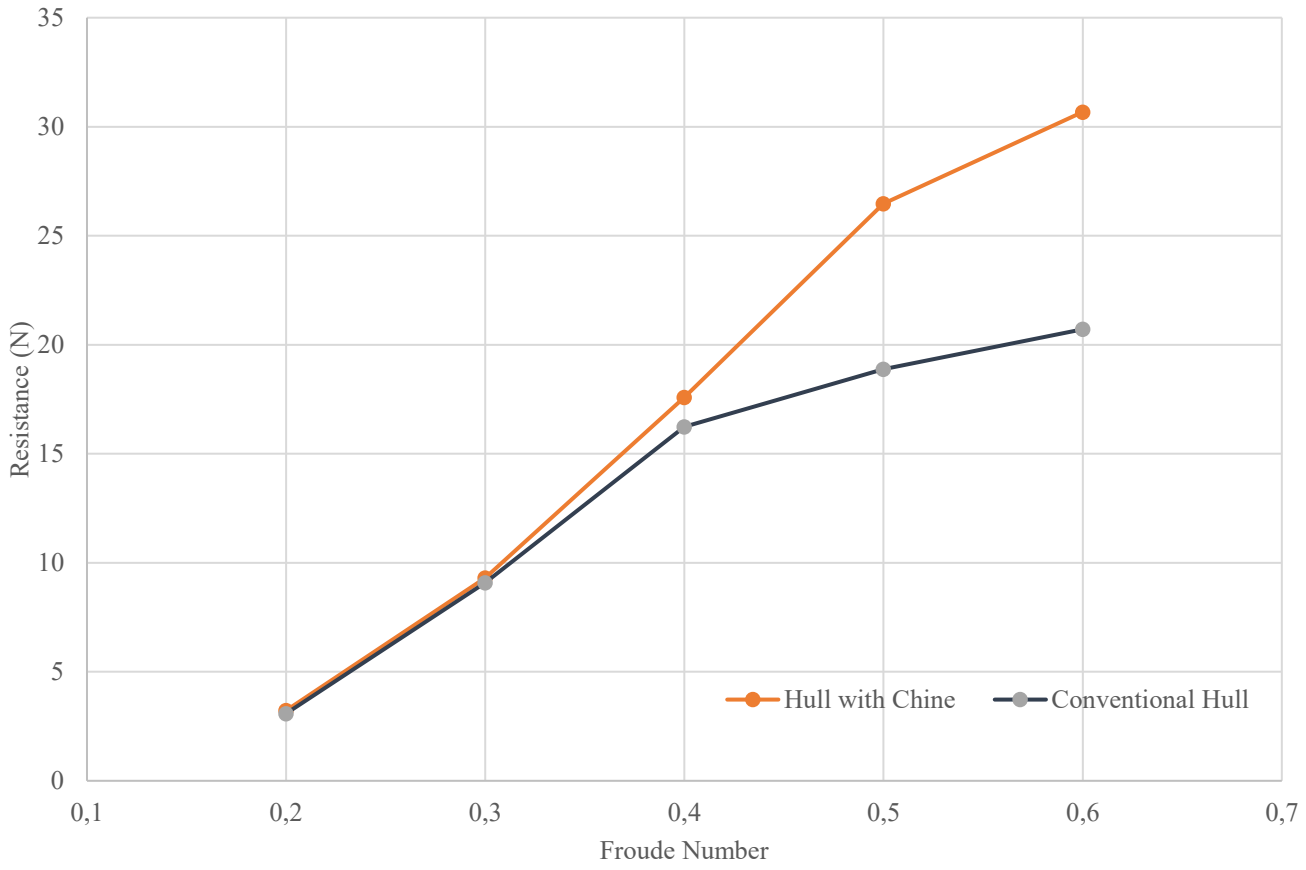

Figure 7. Resistance results: conventional hull vs. hull with chine graph

The results of this study on the resistance of conventional and broadhead hull designs are presented in Table 7 and Figure 8, which show the overall resistance of both hull models based on ship speed, represented by the Froude number Fr. A comparison of the resistance of the Chine hull and the conventional hull is also presented. The chine hull model exhibits higher resistance compared to the conventional hull, with an average difference of approximately 7.69%. This phenomenon can be explained by the smaller wetted surface area of the conventional hull compared with that of the chine hull, and by the chine hull's more effective wave-cutting ability. Regarding the total resistance shown in Figure 8 and Table 7, across all ship-speed conditions, the broadhead hull has lower total resistance than the conventional hull, with an average difference of approximately 7.69%. This indicates that the broadhead hull is more efficient in saving engine power than the conventional hull.

Table 7. Details of the conventional hull and the hull with a wide bow downwards

Froude	Conventional Hull (N)	Hull with a Wide Bow Downwards (N)	Error (%)
0.2	3.09	2.78	-9.94
0.3	9.09	8.56	-6.01
0.4	16.23	14.98	-7.74
0.5	18.88	17.82	-5.59
0.6	20.71	18.81	-9.19

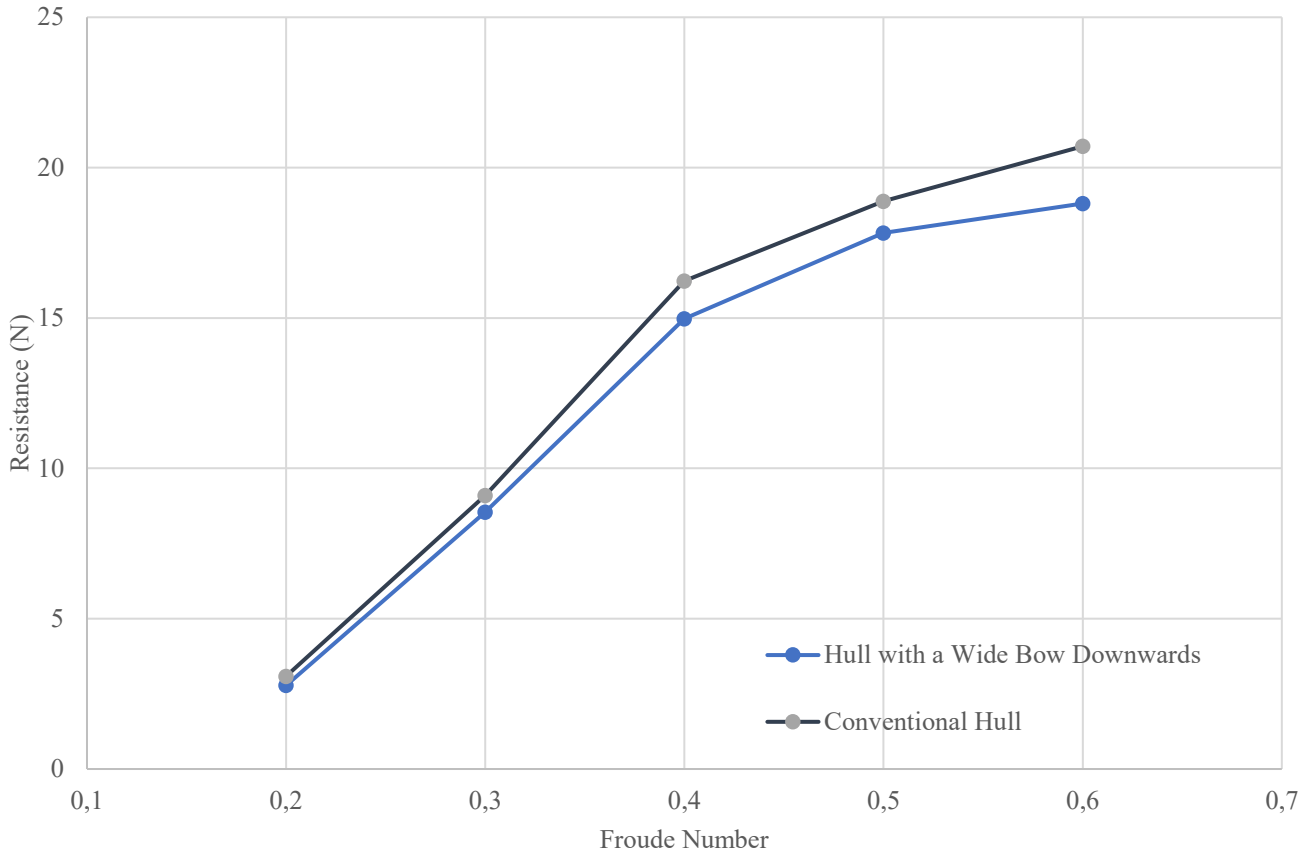

Figure 8. Visualization of the conventional hull vs the hull with a wide bow downwards

Based on the simulation results and analysis of the drag graphs for the three hull types shown in Figure 9, it can be concluded that they exhibit markedly different performance characteristics across their operational speed ranges, as represented by the Froude Number (Fn). Conventional hulls exhibit classic behavior with a very high drag peak (hump) at Fn around 0.4–0.5. This indicates that at medium speeds, vessels with conventional hulls will experience a significant increase in wave drag, leading to inefficient fuel consumption. Therefore, if the vessel frequently operates in this speed range, a conventional hull is not an optimal choice. On the other hand, hulls with chines exhibit a gentler and lower drag curve than conventional hulls, especially after Fn 0.4. This design effectively reduces wave drag and provides better stability and lift at high speeds (Fn > 0.5). Thus, chine hulls are suitable for applications requiring high speeds, such as fast patrol boats or recreational vessels. However, the most interesting results are shown by hulls with a wide, downward-facing bow. In the Fn range of 0.3–0.6, this hull has the lowest resistance of the three. The wide, downward-curving shape of the bow acts like a wedge to push water sideways efficiently, while reducing wave formation at the bow. This makes it very suitable for medium-speed operation.

Based on the graph in Figure 9, it can be explained that at low speeds (Froude Number < 0.4), the three types of hulls, namely, hulls with a wide downward bow, hulls with chines, and conventional hulls, have relatively low drag values and are not significantly different. However, as speeds increase (Froude Number > 0.4), the total drag of the three hulls begins to show a clear difference, where the hull with chines experiences the sharpest increase in drag and becomes the highest due to the wider wetted area due to the presence of chines, thereby significantly increasing the skin supply (frictional resistance). Meanwhile, the hull with a wide downward bow actually shows the lowest drag at high speeds because the shape of the bow that widens downwards cuts through the water more efficiently, reducing wave formation and wave resistance. Conventional hulls are in between, offering balanced performance over a wider speed range.

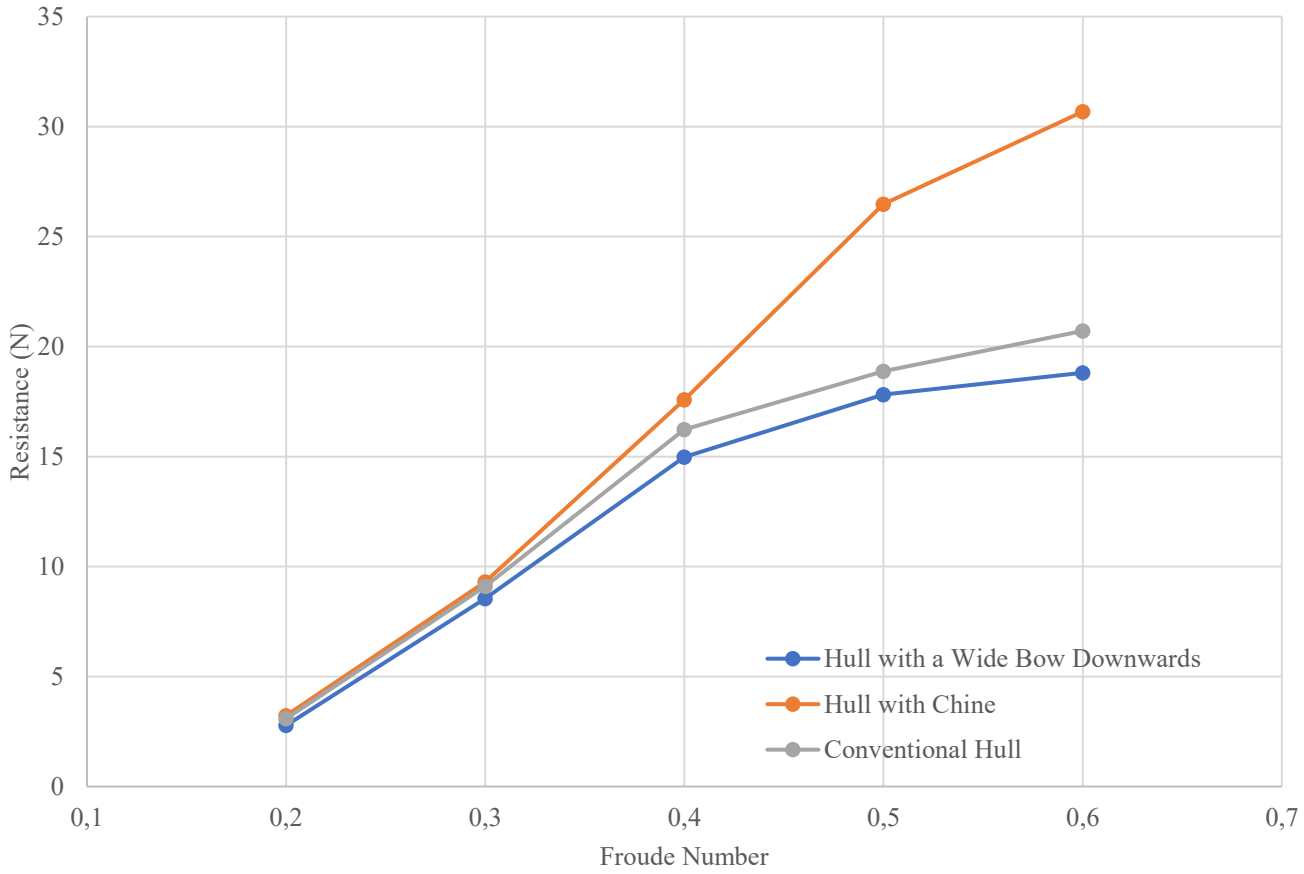

Figure 9. Resistance results of all hull designs

4 Conclusions

This study successfully analyzed the resistance characteristics of three hull variations: conventional, chine, and wide bow downward using a CFD approach based on the RANS equations. Although the simulation results were partially validated against experimental data for the conventional hull (with an average error of 4.25%), this validation does not guarantee the same level of accuracy for the modified hull forms. The numerical results indicate that the wide-bow downward-hull configuration generally produces lower total resistance than the conventional hull, particularly in the medium- to high-speed range (Froude numbers between 0.3 and 0.6), with an average resistance reduction of approximately 7.69%. Conversely, the hull equipped with a chine showed a significant increase in resistance (averaging 20.7%) compared to the conventional design. However, it may offer improved transverse stability due to an increased waterplane area.

However, these findings must be interpreted with caution due to several methodological limitations. The conclusion that the wide-bow downward-hull is superior "at every ship speed" is inaccurate, as the data show it has marginally higher resistance than the conventional hull at the lowest speed tested (Fn 0.2). Furthermore, the simulation methodology contains critical inconsistencies, including a contradiction in the specified turbulence model SST $k-\omega$ and potentially inappropriate boundary conditions, which could affect the reliability of the results. Future work should prioritize methodological consistency, conduct simulations with identical displacement to isolate the pure effect of hull form, and perform direct validation of all hull variations studied to confirm these preliminary findings.

5 Acknowledgement

This research work is supported by DPA FT UNNES Year of 2024 with the number 421.14.3/UN37/PPK.11/2025 and Creativity and Research Club Department of Mechanical Engineering of Universitas Negeri Semarang. Indonesia for helping authors in this research.

References

1. N. K. Rijal, "Kepentingan Nasional Indonesia dalam Inisiasi ASEAN Maritime Forum (AMF)," *Indones. Perspect.*, vol. 3, no. 2, pp. 159-179, 2019 (*In Indonesian*).
2. M. C. Ricklefs, *A History of Modern Indonesia since c. 1200*. London: Palgrave, 2011.
3. S. Hutajulu, R. Aprilla, and H. Pardi, "Peran Scrubber Pada Bahan Bakar Rendah Sulfur Dalam Mengatasi Polusi Udara Maritim," *Politek. Bumi Akpelni Semarang*, vol. 25, no. 2, pp. 117-122, 2023 (*In Indonesian*).
4. KESDM, *Kapal Survei Geomarin III Sebagai Sebuah Jawaban.* Jakarta: Ministry of Energy and Mineral Resources Indonesia, 2009 (*In Indonesian*).
5. B. Wahyudi and I. Fachruddin, "Analisis Daya dan Biaya Penggunaan Low Sulfur Fuel Oil (LSFO) dengan High Sulfur Fuel Oil (HSFO) dilengkapi Scrubberpada Kapal Niaga," *Din. Bahari*, vol. 1, no. 1, pp. 31-37, 2020 (*In Indonesian*).
6. A. Farid and I. G. N. Sumanta Buana, "Model Perancangan Konseptual Armada Supply Vessel Untuk Mendukung Operasi Rig Dan Offshore Platform (Studi Kasus : Wilayah Lepas Pantai Utara Jawa Timur)," *J. Tek. ITS*, vol. 1, no. 1, pp. 33-37, 2012 (*In Indonesian*).
7. A. A. Afdhani, *Analisis pelaksanaan kerja dalam pelayanan anchor handling di deck ahts*. Makassar: Politeknik Ilmu Pelayaran Makassar, 2024 (*In Indonesian*).
8. D. Kim, J. M. Seo, S. Ahn, and H. Lee, "Effectiveness of Dispersants for Very-Low-Sulfur Fuel Oil," *J. Korean Soc. Mar. Environ. Saf.*, vol. 27, no. 1, pp. 113–118, 2021.
9. N. Sharma, *IMO 2020 sulfur cap: green investment in shipping industry*. Malmö: World Maritime University, 2019.
10. C. K. Wachjoe, H. Zein, Y. Supriyanti, T. M. Gantina, A. Kurniasetiawati, And P. Marenshaputri, "Pengurangan Pencemaran Udara berdasarkan Konsep Pelabuhan Hijau," *Elkomika J. Tek. Energi Elektr. Tek. Telekomun. Tek. Elektron.*, vol. 8, no. 2, article no. 252, 2020 (*In Indonesian*).
11. A. Ramadhan, H. D. Armono, and K. Sambodho, *Aplikasi Konsep Ecoport di Pelabuhan Tanjung Perak, Surabaya*. Surabaya: Institut Teknologi Sepuluh Nopember, 2016 (*In Indonesian*).
12. A. Fitriadhy, N. S. Rizat, A. R. A. Razak, S. F. Abdullah, F. Mahmuddin, and A. Kurniawan, "Optimization Modelling of a Catamaran Hull Form towards Reducing Ship's Total Resistance," *CFD Lett.*, vol. 14, no. 4, pp. 67–79, 2022.
13. T. K. Le, N. Van He, N. Van Hien, and N. T. Bui, "Effects of a bulbous bow shape on added resistance acting on the hull of a ship in regular head wave," *J. Mar. Sci. Eng.*, vol. 9, no. 6, article no. 559, 2021.
14. S. Zhang, Q. Wu, J. Liu, S. Li, and H. Yasukawa, "Impact of bulbous bow shapes on hydrodynamic derivatives due to hybrid drifting and circular motion tests," *Ocean Eng.*, vol. 289, no. 7, article no. 116182, 2023.
15. G. Philippe, S. L. Pallec, and Y. Floch, *Why Consider Inverted Bows on Military Ships? Or why Not?*. Paris: Association Technique Maritime et Aéronautique, 2018.
16. J. K. White, S. Brizzolara, and W. Beaver, "Effect of Inverted Bow on the Hydrodynamic Performance of Navy Combatant Hull Forms," Massachusetts: Massachusetts Institute of Technology, 2015.
17. A. Nazemian and P. Ghadimi, "Automated CFD-based optimization of inverted bow shape of a trimaran ship: An applicable and efficient optimization platform," *Sci. Iran.* , vol. 28, no. 5, pp. 2751-2768, 2021.
18. ITTC, *Practical Guidelines for Ship CFD Applications*. Zürich: International Towing Tank Conference (ITTC) Association, 2011.
19. S. Samuel, S. Yulianti, P. Manik, and A. Fathuddiin, "A study of interceptor performance for deep-v planing hull," *IOP Conf. Ser. Earth Environ. Sci.*, vol. 1081, no. 1, article no. 012004, 2022.
20. Samuel, R. K. Praja, D. Chrismianto, M. L. Hakim, A. Fitriadhy, and A. Bahatmaka, "Advancing Interceptor Design: Analyzing the Impact of Extended Stern Form on Deep-V Planing Hulls," *CFD Lett.*, vol. 16, no. 5, pp. 59-77, 2024.
21. U. Budiarto, S. Samuel, A. A. Wijaya, S. Yulianti, Kiryanto, and M. Iqbal, "Stern Flap Application on Planing Hulls to Improve Resistance," *Int. J. Eng. Trans. C Asp.*, vol. 35, no. 12, pp. 1184–1191, 2022.
22. T. J. Chung, *Computational Fluid Dynamics*. Huntsville: Cambridge University Press, 2010.
23. K. M. Almohammadi, D. B. Ingham, L. Ma, and M. Pourkashan, "Computational fluid dynamics (CFD) mesh

independency techniques for a straight blade vertical axis wind turbine," *Energy*, vol. 58, pp. 483-493, 2013.
24. A. Chandra, C. Kirana, A. Bahatmaka, D. Malsyage, J. H. Cho, and S. O. Ttum, "Analysis of Variations in Bow Design and Vessel Speed on the Response Amplitude Operator (RAO) of a Crew Boat Using Computational Fluid Dynamics (CFD)," vol. 24, no. 9, pp. 136-150, 2025.
25. P. G. Tucker, *Advanced Computational Fluid and Aerodynamic*. Cambridge: Cambridge University Press, 2016.
26. A. Bahatmaka, D. F. Fitriyana, S. Anis, A. Y. Maulana, M. Tamamadin, S. W. Lee, and J. H. Cho, "Analytical Review of Numerical Analysis in Hydrodynamic Performance of the Ship: Effect to Hull-Form Modifications," *Mek. Maj. Ilm. Mek.*, vol. 23, no. 1, pp. 54-63, 2024.
27. M. Tabatabaian, *CFD module: Turbulent Flow Modeling (Multiphysics Modeling Series)*. Boston: Mercury Learning and Information, 2015.
28. S. Samuel, S. T. F. Evan, A. Trimulyono, and M. Iqbal, "An analysis of the effect of the bow entrance angle on ship resistance," *SINERGI*, vol. 26, no. 2, pp. 223-228, 2022.
29. S. Samuel, A. Wicaksono, W. A. Kurniawan, E. S. Hadi, T. Tuswan, A. Trimulyono, and M. Muryadin, "Investigation of An Inverted Bow on Frigate Hull Resistance," *J. Appl. Fluid Mech.*, vol. 17, no. 1, pp. 136-147, 2024.
30. D. Savitsky, "Hydrodynamic Design of Planning Hulls," *Mar. Technol. SNAME News*, vol. 1, no. 4, pp. 71-95, 1964.
31. S. Brizzolara and F. Serra, "Accuracy of CFD codes in the prediction of planing surfaces hydrodynamic characteristics," *in the International Conference of Marine Research and Transportation*, Naples, Italy, 2007.